





Specific heat studies of the phase transitions in multiferroic $\text{Sr}_{1-u}\text{Ba}_u\text{Mn}_{1-y}\text{Ti}_y\text{O}_3$ system ($0 \leq u \leq 0.65$, $0 \leq y \leq 0.1$)

J. Wieckowski , A. Szewczyk ^{*}, M. U. Gutowska , and B. Dabrowski 

Institute of Physics, Polish Academy of Sciences, Aleja Lotników 32/46, PL-02668 Warsaw, Poland



(Received 6 August 2024; revised 7 May 2025; accepted 3 June 2025; published 20 June 2025)

Specific heat studies of the $\text{Sr}_{1-u}\text{Ba}_u\text{Mn}_{1-y}\text{Ti}_y\text{O}_3$ system polycrystalline samples performed by the relaxation and DSC methods over the temperature range 2–450 K are reported. Anomalies accompanying the antiferromagnetic-paramagnetic and ferroelectric-paraelectric phase transitions were measured. The system studied is a promising multiferroic material of the first type, in which a strong coupling between the magnetic and electric systems, related probably to the fact that the same Mn^{4+} ions are responsible for the two orderings, appears. Analysis of the specific heat anomaly at the magnetic transition was done using the advanced theory of the continuous transitions, in which the presence of higher order terms in the free energy is considered, and the parameters of the critical behavior of the system were estimated. The shape of this anomaly suggests that arguably, despite earlier predictions, the transition loses the continuous character and becomes the first-order process for the Ti-containing samples. For majority of the compositions, the anomaly accompanying the first-order high-temperature ferroelectric transition was found to be smeared and not well pronounced, which was tentatively ascribed to a wide temperature range of coexistence of the para- and ferroelectric phases and a small difference between entropies of both phases.

DOI: [10.1103/hn32-kxms](https://doi.org/10.1103/hn32-kxms)

I. INTRODUCTION

By definition [1], “multiferroics” are materials which display several coexisting long-range orderings, often of magnetic and dielectric nature. Usually one distinguishes [2,3] the first type or “proper” multiferroics, in which the long-range orderings appearing at separated temperatures are weakly coupled or fairly independent of each other, and the second type or “improper” ones, in which the orderings are strongly coupled or even the appearance of a one ordering is induced by the appearance of the second one, as, for example, in TbMnO_3 [4–6]. The latter multiferroics, especially magnetoelectrics, have attracted great interest among researchers because they could find numerous applications, including electrically controlled magnetic memories, electric amplifiers of magnons, magnetic field sensors, writing/reading heads of hard drives, and others [7].

Presumably, the group of ABO_3 oxides having a crystalline structure of a slightly deformed perovskite (where A = alkaline or rare earth ion or a set of such ions and B = transition metal ion or a set of such ions), among which there are more than 100 compositions showing magnetic orderings and a similar number of compositions showing a ferroelectric ordering, should be promising set for obtaining many second-type

multiferroic compounds. However, there are only a few known multiferroic compositions of this group. It is believed that the scarceness is due to the crystalline structure of these materials, in which each B ion is located inside octahedral coordination made of six oxygen ions. In the ideal perovskite structure, the $B\text{-O}_6$ octahedra are relatively rigid and densely packed complexes, forming a simple corner-shared cubic lattice, whereas the A ions locate in free space between the octahedral complexes. In many materials, due to misfit of the atomic radii of the A , B , and O^{2-} ions, small deformations and rotations of the $B\text{-O}_6$ complexes are observed, which lower the crystal symmetry from the cubic $Pm\bar{3}m$ one of the ideal perovskite to a tetragonal, rhombohedral, or orthorhombic one; however, the general integrity of the perovskite-based network remains unchanged.

Calculations described in [8], based on the density functional theory, showed that it is energetically favorable for the B ion with the empty d shell to shift from the center of the oxygen octahedron towards one of the apical oxygen ions (or towards three oxygen ions) and to form a strong covalent bond with this particular oxygen (or oxygens) at the expense of weakening the bonds with other oxygens. In such a case, only the bonding state of lower energy is occupied. This process breaks the inversion symmetry of the distribution of positive and negative ionic charges and results in the appearance of a nonzero spontaneous electric polarization and, in some cases, in the appearance of the ferroelectric ordering. On the other hand, if B is a “magnetic” ion, i.e., if it has at least one electron on the d shell, the antibonding state of higher energy also is occupied, which results in reducing the energy gain related to the shift of the B ion from the oxygen octahedron center. Apart from this factor, if the B ion has a few electrons on the d

^{*}Contact author: szewc@ifpan.edu.pl

shell, the exchange interactions between them, preferring the parallel orientation of their spins and being the physical basis for the first Hund's rule (thus called "the Hund's coupling"), must be taken into account. As the result (illustrated in Fig. 2 of Ref. [8]), the shift of such a B ion from the center of the oxygen octahedron becomes inconvenient energetically. Thus, the inversion symmetry is preserved and the material displays no spontaneous dielectric polarization. However, some kinds of a magnetic ordering can appear in such compounds.

In this context, researchers intensively seek for methods of overcoming this incapability and obtaining the multiferroic perovskites. For example, the following methods were described in the literature [8]: (i) partial replacement of magnetic B ions with nonmagnetic ones, which resulted in discovering the $\text{PbFe}_{0.5}\text{Nb}_{0.5}\text{O}_3$ multiferroic; (ii) relating magnetic properties to the B sublattice and the ferroelectric properties to the A sublattice occupied by ions having, like Bi, a so-called lone pair of s electrons, which is the origin of multiferroic properties of intensively studied BiFeO_3 and BiMnO_3 compounds; and (iii) synthesizing materials, like TbMnO_3 [4–6], in which, mainly due to the Dzyaloshinskii-Moriya interactions [9], an incommensurate noncentrosymmetric spiral magnetic structure and, simultaneously, displacements of magnetic and oxygen ions from their "normal" symmetric positions, producing nonzero electric polarization, appear. However, it was found that, with the exception of the third group, in all such materials, the magnetic and electric order parameters are coupled rather weakly.

The new method of obtaining multiferroic perovskites proposed in Ref. [10] was based on the idea that (i) much stronger magnetoelectric coupling could be achieved if the same ions were responsible for the electric and magnetic orderings and (ii) stretching the oxygen octahedra by the chemical tensile stress produced by replacement of small A ions with larger ones could result in producing more free space around the magnetic ions, e.g., Mn^{4+} , located within the octahedra, and in making the displacement of the magnetic ions from the centers of the octahedra energetically favorable, which would lead to the appearance of the spontaneous polarization. This idea was verified for the $\text{Sr}_{1-u}\text{Ba}_u\text{MnO}_3$ system [10,11], by replacing the smaller Sr^{2+} ions with the larger Ba^{2+} ones. It was found that for $u \geq 0.45$ the structural transition to the ferroelectric phase appears at high temperatures, $T_C \sim 400$ K, and then, on lowering temperature, at $T_N \sim 200$ K, the phase transition to the antiferromagnetic phase of the type G takes place, and, thus, the multiferroic state is gained. Unfortunately, it turned out that the system is not the ideal one, because it shows too high electric conductivity, which prohibits a direct measurement of the spontaneous polarization, and the structural deformation resulting in the spontaneous polarization decreases significantly at the point of magnetic transition. Nevertheless, this reduction of deformation proves the existence of a desired strong coupling between the magnetic and electric orderings, which makes the $\text{Sr}_{1-u}\text{Ba}_u\text{MnO}_3$ system a good initial composition for further investigations. The continued studies of the $\text{Sr}_{1-u}\text{Ba}_u\text{MnO}_3$ system established the synthesis procedures allowing for increasing the limits of Ba substitution and the partial replacement of Mn with Ti, which resulted in stronger ferroelectric deformation and higher T_C [12]. Detailed studies of homogeneity and mag-

netic properties of the obtained compositions were reported in Ref. [12]. The recent studies of the local atomic and magnetic structures using x-ray and neutron pair distribution function analysis, polarized neutron scattering, and muon spin relaxation techniques showed presence of the nanoscale tetragonal distortions in the paraelectric phase and the short-range antiferromagnetic correlations in the paramagnetic state over the wide temperature ranges [13].

The present studies were aimed at a closer analysis of antiferromagnetic and ferroelectric phase transitions appearing in the $(\text{Sr,Ba})(\text{Mn,Ti})\text{O}_3$ compounds and of the critical behavior near the antiferromagnetic transition. Specifically, we wanted to verify the suggestion made in Ref. [12] that the substitution of Mn with Ti does not change the second-order character of the magnetic transition. Since it is known [12] that at the magnetic transition point the structural deformation responsible for the spontaneous electric polarization decreases substantially, it is obvious that this transition also influences the lengths and angles of the Mn-O-Mn bonds, and consequently, the strength of exchange interactions. As was shown in Ref. [14], such an effect, when sufficiently strong, can change the order of the transition from the second to the first one.

Since the magnetic ordering appearing at the low-temperature transition to the multiferroic state has the antiferromagnetic character and the high-temperature ferroelectric-paraelectric phase transition weakly influences magnetic properties of the system, magnetic measurements are not appropriate for studying these transitions. As an alternative, the measurements of specific heat are more suitable and informative. Moreover, the sign and value of the specific heat critical exponent α depend strongly on the character of magnetic structure of the system studied [15]. Thus, the specific heat measurements were chosen as the main experimental method of the present studies, and detailed measurements of this parameter for a series of $(\text{Sr,Ba})(\text{Mn,Ti})\text{O}_3$ compositions as well as the detailed analysis of the shape of the specific heat anomalies accompanying the antiferromagnetic phase transitions were performed.

II. EXPERIMENT

The almost single-phase polycrystalline $\text{Sr}_{1-u}\text{Ba}_u\text{Mn}_{1-y}\text{Ti}_y\text{O}_3$ samples with $u = 0\text{--}0.65$ and $y = 0.0\text{--}0.1$ were synthesized from stoichiometric mixtures of BaCO_3 (99.9% pure), SrCO_3 (99.99%), MnO_2 (99.95%), and TiO_2 (99.99%) with methods described in detail in Refs. [11] and [12]. In short, the synthesis of the perovskite compounds studied here is a difficult task involving repeated firing under increasingly reducing conditions at high temperatures to achieve the required chemical compositions surviving beyond ordinary solubility limits by removing the hexagonal second phases of the similar compositions, which normally form in the oxygen containing atmospheres. The procedure is followed by the oxidation of the oxygen-deficient perovskites to the full oxygen content at lower temperatures without decomposition; however, it could lead in some cases to the presence of small amounts of second phases and the chemical compositional inhomogeneities.

For the present specific heat measurements, the following compositions were chosen: $y = 0$ and $u = 0, 0.43$, and 0.45 ; $y = 0.02$ and $u = 0.5$; $y = 0.06$ and $u = 0.45, 0.5, 0.55, 0.6$, and 0.65 ; and $y = 0.1$ and $u = 0.5$.

Two methods of specific heat measurement were used. For the temperature range $2 \leq T \leq 400$ K, the studies were done with the relaxation method using the specific heat (HC) option of the PPMS system (made by Quantum Design). The measurements were performed for zero and several fixed values of the external magnetic field, B , up to 9 T. Typically, in the vicinity of phase transitions and below 15 K, the experimental points were measured every 0.2 or 0.5 K, whereas outside these regions, every 1, 2, or 3 K. To maintain the readability of all figures presented below, only the limited numbers of experimental points are denoted with the symbols. The high accuracy (to 2%) of the determined absolute values of the specific heat for T smaller than ~ 250 K is the main advantage of this method. Above ~ 250 K the heat transfer between the calorimeter and the environment via radiation increases substantially (it is proportional to T^4) and dominates the other mechanisms (convection and conduction), which results in increased noise and deterioration of the accuracy of the determined absolute specific heat values to ca. 5%. Moreover, the inherent property of the relaxation method, i.e., the necessity of applying the measuring heat pulses increasing the sample temperature by ca. 2% of T , results in rounding the specific heat maxima accompanying phase transitions and makes this technique not optimally suited for determining the critical exponent α .

Thus, for measurements in the temperature range $100 < T < 450$ K, the differential scanning calorimetry system (DSC; made by TA Instruments) was used. The DSC method, in which changes of heat capacity are measured during the temperature sweep with a fixed speed (usually from 1 to 10 K/min), is very precise and effective in detecting all anomalies of the specific heat, usually those related to phase transitions. However, it does not allow one to determine accurately the absolute specific heat values.

In this context, by combining the two methods mentioned above we were able to study both the magnetic phase transition appearing in the range $130 < T < 230$ K and the ferroelectric transition appearing in the range $\sim 350 < T < \sim 400$ K. Furthermore, using the fact that the temperature ranges of applicability of the two measuring systems overlapped within the range $\sim 100 < T < \sim 350$ K we were able to shift the absolute specific heat values reported by the DSC system to the values determined by the relaxation method and thus to determine more reliably the absolute specific heat values for the high-temperature range $T > 300$ K.

Additionally, magnetization measurements were performed to verify the accuracy of the measured transition temperatures using the vibrating sample magnetometer (VSM) option of the PPMS system.

III. RESULTS

Specific heat, C , measured as a function of temperature in zero magnetic field for all compositions studied is presented in Fig. 1. One can easily notice that the most pronounced anomaly accompanies the phase transition, which was

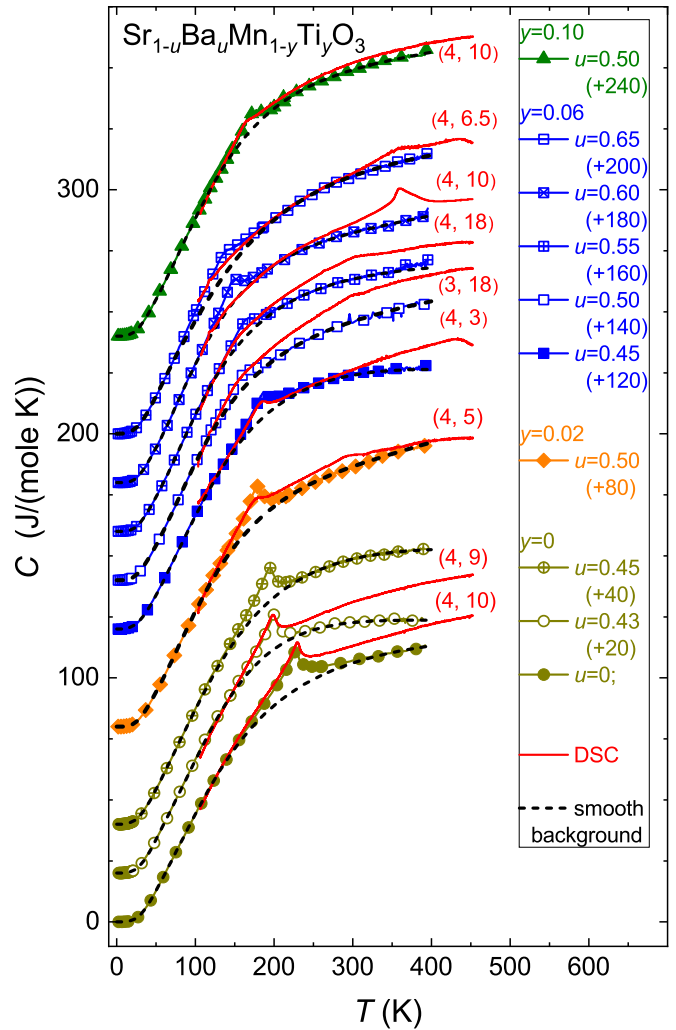


FIG. 1. Specific heat of the $\text{Sr}_{1-u}\text{Ba}_u\text{Mn}_{1-y}\text{Ti}_y\text{O}_3$ compositions as a function of temperature. Curves measured with the PPMS are denoted by symbols and plotted in dark yellow, orange, blue, and green, for $y = 0, 0.02, 0.06$, and 0.10 , respectively. On each PPMS curve, there are superimposed (i) the smooth background, mimicked with Eq. (1), plotted with the dashed black line and (ii) the dependence measured with the DSC method, plotted with the solid red line. In the legend, at the symbols denoting the PPMS data, the u content, and, in parentheses, the value by which all curves for this composition are shifted along the vertical axis are given. At each DSC curve the heating rate at which it was registered, in K/min, and the value in J/(mole K) by which the DSC curve was shifted with respect to the PPMS data to get the more reliable absolute specific heat values are given in parentheses.

identified earlier [10–12] as the transition from the paramagnetic to the antiferromagnetic phase of type G. It was found that replacement of both Sr with Ba and Mn with Ti lowers the Néel temperature, T_N , from 228 K for the pure SrMnO_3 to 135 K for the $\text{Sr}_{0.35}\text{Ba}_{0.65}\text{Mn}_{0.94}\text{Ti}_{0.06}\text{O}_3$ composition; see Fig. 2 and Table II below. In all cases, the specific heat anomaly is wide, smeared over the temperature range of 110–220 K depending on the composition. We attribute the smearing to small inhomogeneities of the chemical composition of particular samples and to small deviations of the actual

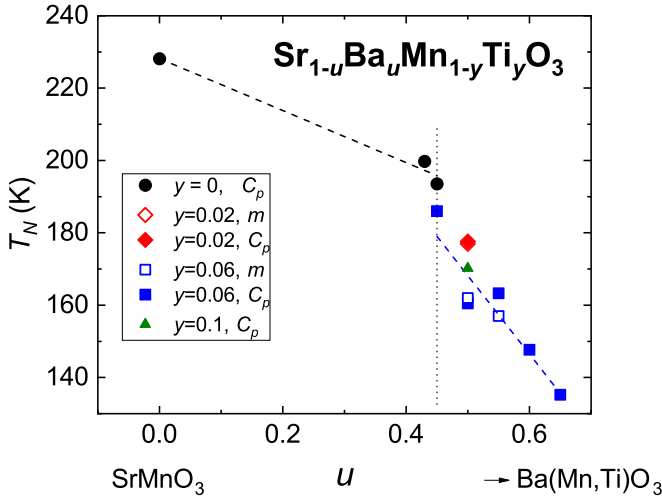


FIG. 2. Néel temperatures of the $\text{Sr}_{1-u}\text{Ba}_u\text{Mn}_{1-y}\text{Ti}_y\text{O}_3$ system, T_N , as a function of u . The arrow indicates a hypothetical composition to which the system evolves with increasing u . Full and empty symbols denote, respectively, the temperature corresponding to maximum of the specific heat anomaly and the data from magnetization measurements.

oxygen stoichiometry from the value “3,” which could appear due to, mentioned above, technological difficulties in synthesizing these compositions.

In order to assess the usefulness of the studied system for potential applications, we verified whether a desired strong influence of the external magnetic field on the magnetic ordering appears in it. Usually, in the case of antiferromagnetic transitions, the uniform external magnetic field lowers the transition temperature and sharpens the specific heat anomaly that it accompanies. However, the specific heat measurements performed for the $(\text{Sr,Ba})(\text{Mn,Ti})\text{O}_3$ system for several fixed values of the magnetic field, B , up to 9 T showed that the influence of the magnetic field on the antiferromagnetic transition is always negligible, even for $B = 9$ T. As an example, this effect is illustrated in Fig. 3, where the specific heat of the $u = 0.6$ and $y = 0.06$ composition measured as a function of temperature for several fixed B values is presented. This is rather a surprising effect because the molecular field for the studied system, roughly estimated based on the T_N value, is on the order of 35–60 T and the external field of 9 T constitutes its noticeable fraction. We presume that the influence of B on the transition seems to be negligible because of the large widths of the anomalies related to the antiferromagnetic transition. In this context, the studied system is not especially promising for applications.

Unlike the anomalies at the antiferromagnetic transitions, the specific heat anomalies at the ferroelectric transitions are, practically, invisible in the PPMS data and are smeared and not well pronounced in the DSC results (Fig. 1). We attribute this to the fact that these transitions are of the first order and, as the x-ray studies showed [12], the temperature range of coexistence of para- and ferroelectric phases is relatively wide (~ 60 K), which smears the specific heat anomaly related to the ferroelectric transition. Moreover, we assume tentatively that the difference between the entropies of both phases can be

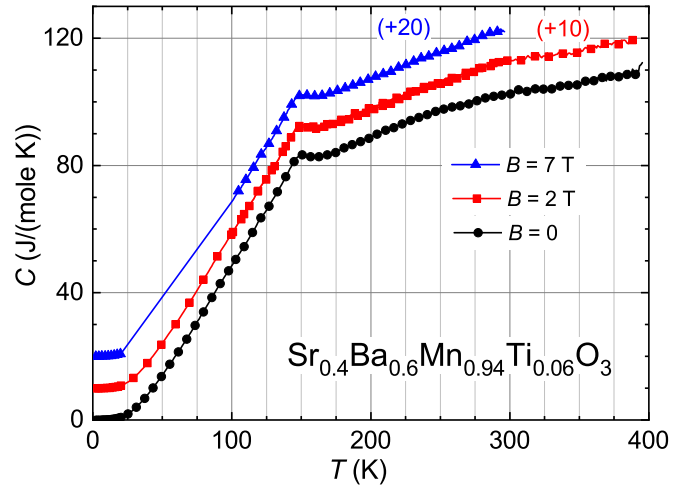


FIG. 3. Temperature dependence of the specific heat, C , of $\text{Sr}_{0.4}\text{Ba}_{0.6}\text{Mn}_{0.94}\text{Ti}_{0.06}\text{O}_3$ in the presence of an external magnetic field, B . To maintain legibility, only selected measured points are indicated by symbols, and the curves are shifted along the vertical axis by the values given in parentheses.

rather small, which would result in small height of the specific heat anomaly.

IV. ANALYSIS

To investigate the anomalies accompanying the antiferromagnetic phase transition it was necessary to extract the largest contribution to the measured specific heat, i.e., the noncritical smooth background, composed of the phonon and magnon contributions. Since in the case of weakly anisotropic antiferromagnetic materials, the dispersion relation for the magnons ($\omega \sim k$), the magnon and phonon contributions to specific heat depend on temperature in the same way, and separating them is not trivial. Thus, to mimic the effective smooth contribution to the specific heat we used the following, frequently applied expression [16,17], consisting of a mixture of the Debye and Einstein models:

$$C_s(T) = \left[\frac{3n_D k_B N_A}{(1 - \alpha_D T)} \left(\frac{T}{\theta_D} \right)^3 \int_0^{\theta_D/T} \frac{t^4 e^t}{(e^t - 1)^2} dt + \frac{k_B N_A}{(1 - \alpha_E T)} \sum_{i=1}^{n_O} n_i \left(\frac{\theta_i}{T} \right)^2 \frac{e^{\theta_i/T}}{(e^{\theta_i/T} - 1)^2} \right]. \quad (1)$$

The first term of (1) describes the contribution arising from the n_D branches approximated by the Debye model with the Debye temperature θ_D , and the second term represents the contribution arising from the n_O optical branches described by the Einstein model. The Einstein temperature θ_i and the number n_i of modes are ascribed to each of the n_O optical branches. The effect of lattice expansion can be considered in the way proposed in Ref. [18], i.e., by introducing the factor $1/(1 - \alpha_i T)$ for each branch. In the present analysis we introduced a simplification, consisting in considering only two α_i coefficients, namely, the one for the Debye branches, α_D , and the other one, α_E , for the Einstein branches. Satisfactory

TABLE I. Fitting parameters used for modeling the smooth specific heat background of $\text{Sr}_{1-u}\text{Ba}_u\text{Mn}_{1-y}\text{Ti}_y\text{O}_3$ compositions.

Sample		θ_D	α_D	α_E	θ_1	n_1	θ_2	n_2
u	y	(K)	(1/K)	(1/K)	(K)		(K)	
0.5	0.1	231.7	9.8×10^{-4}	-9.2×10^{-4}	256	3	514	11
0.65	0.06	223	-2.8×10^{-3}	1.6×10^{-4}	268	5	581	8
0.6	0.06	294.6	1.05×10^{-3}	-8.79×10^{-4}	177.7	2	447.3	10
0.55	0.06	247	-11.4×10^{-3}	-8×10^{-5}	205.2	3	446.4	11
0.5	0.06	253	-4.15×10^{-3}	3.14×10^{-4}	191	2	430	10
0.45	0.06	230.7	-4×10^{-3}	-5.5×10^{-4}	277	5	550	11
0.5	0.02	260	1.14×10^{-3}	-6.5×10^{-4}	208.9	2	474.3	10
0.45	0	242	-3.9×10^{-4}	-5.16×10^{-4}	265	4	554	11
0.43	0	260	9×10^{-4}	-5.06×10^{-3}	267.3	5	612	23
0	0	267	-4.8×10^{-3}	1.9×10^{-5}	246.9	4	534.3	10

approximation of the smooth specific heat background for each composition has been obtained by taking $n_D = 3$ and $n_O = 2$, and treating θ_D , n_i , θ_i , α_D , and α_E as the fitted parameters. The modeled smooth backgrounds for all the compositions studied are plotted in Fig. 1 with the dashed lines. The values of fitted parameters for which the best descriptions of the backgrounds were achieved are collected in Table I. Since the lattice specific heat is the value summarizing contributions of all phonon modes it is weakly sensitive to particularities of the phonon spectrum. Thus, the fitted parameter values have the meaning of mathematical parameters only, and their relation to the real physical parameters is qualitative only. For example, we can assume that the Debye temperature of the compositions studied is of the order of 250 ± 50 K. Thus, uncertainty of the particular fitted parameters was not estimated. The specific heat anomalies, $C_M(T)$, related to the magnetic phase transition were derived by subtracting the modeled smooth backgrounds from the measured temperature dependences of the specific heat (see Fig. 4). As mentioned above, these anomalies are smeared over the wide temperature ranges, and thus, they could not be analyzed in frames of the basic theory of critical phenomena, in which one assumes that the critical behavior given by a single power function appears when the parameter $\tau = (T - T_N)/T_N$ takes the values $|\tau| \leq 10^{-3}$. Apart from the wide temperature spread of the anomalies, analysis of their real shape within the critical range $|\tau| \leq 10^{-3}$ was, in practice, impossible because they were measured by means of the relaxation method. As discussed previously, in this method, during the measurement process a measuring heating pulse, increasing the sample temperature by the value of the order of 2% of the actual T value, is applied. Thus, the specific heat value assigned to the $T + (2\%T/2)$ temperature is, in fact, the value averaged over the temperature range from T to $T + 2\%T$, which results in “rounding” the anomalies measured for $|\tau| \leq 10^{-3}$.

Therefore, following Refs. [15,19,20], it was assumed that for the compositions studied, the more advanced theory of critical phenomena, taking into account the presence of higher order terms in τ in the expression for the free energy, essential for $|\tau| \geq 10^{-3}$, must be applied. According to this theory, the critical behavior of the specific heat can be represented in the

form

$$C_M(T) = \frac{B}{\alpha} \left[\left| \frac{T}{T_N} - 1 \right|^{-\alpha} - 1 \right] \left[1 + E \left| \frac{T}{T_N} - 1 \right|^x \right] + D, \quad (2)$$

which differs from the classical one by the presence of the term in the second parentheses.

In fact, some authors, e.g., [20,21], instead of modeling the smooth regular background, e.g., using Eq. (1), prefer to take it into account by adding to Eq. (2) a linear term of the form $D_1 + FT$, with D_1 and F being constant values. However, we believe that for the anomalies smeared over such a large temperature range as in the present case, modeling the smooth background by (1) is more appropriate than a linear approximation.

We verified that for the system studied the best description of the experimental anomalies with (2) is achieved for the exponent $x = 0.44$, and this value was used in the further analysis. This result is consistent with earlier papers (e.g., [22]), presenting similar analysis, which showed that for all real physical systems studied until now, the best description can be achieved by taking the value $x \simeq 0.5 \pm 0.2$.

The preliminary calculations showed that for describing the maximum appearing at the Néel temperature for all the compositions, the negative value of the exponent α must be chosen, which is reasonable, because negative α values are predicted also in some theoretical models. For example, the $\alpha = -0.08 \pm 0.04$ value is predicted theoretically for the Heisenberg model [23]. It is important to note that for the negative α values, specific heat does not diverge but shows a finite maximum at the transition point, and hence, the $C_M(T)$ function must be continuous at T_N . Thus, if we denote the parameters of the function (2) with the superscript “−” for $\tau < 0$, i.e., for $T < T_N$, and with the superscript “+” for $\tau > 0$, i.e., for $T > T_N$, the continuity requirement leads to the relation

$$D^+ = D^- + \frac{B^+ - B^-}{\alpha}. \quad (3)$$

Next, we treated α , B^- , B^+ , E^- , E^+ , D^- , and T_N as fitted parameters and matched the dependence (2) to the experimental data for a rather wide temperature range around the

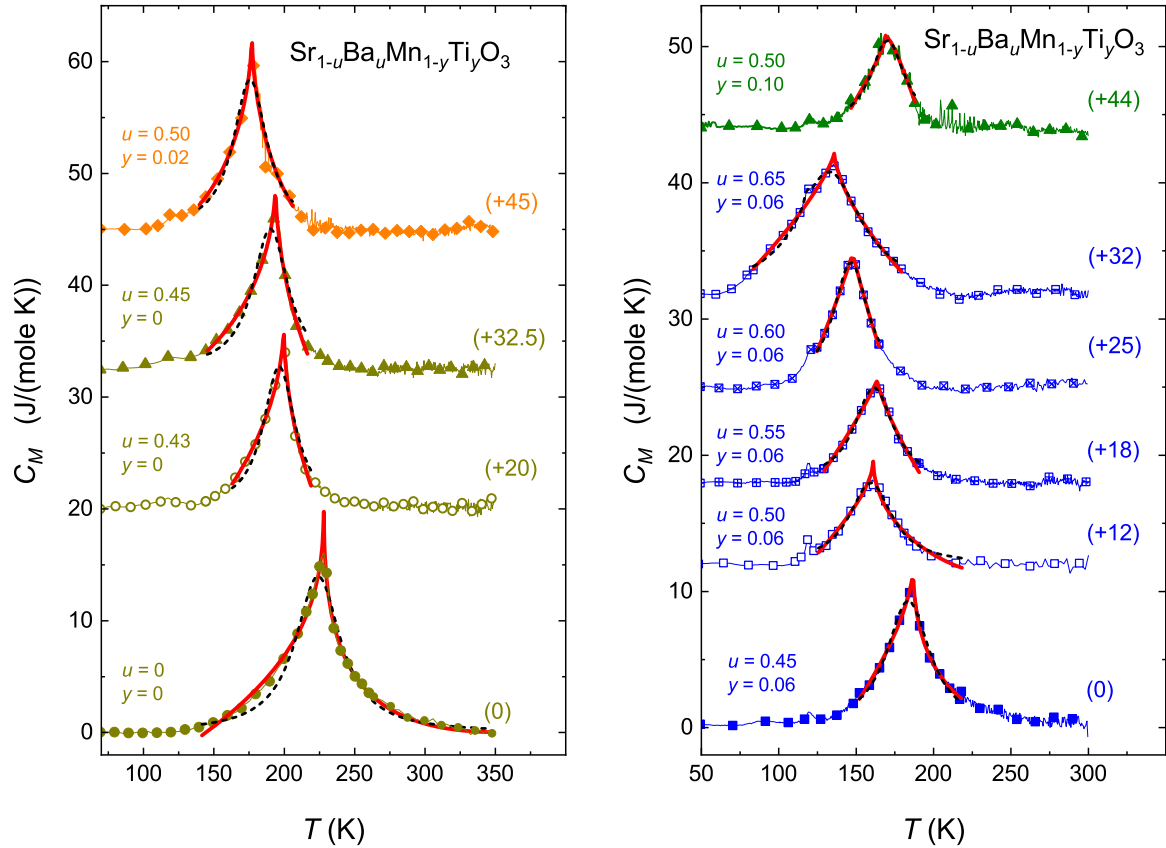


FIG. 4. Specific heat anomalies related to the antiferromagnetic phase transition appearing in the $\text{Sr}_{1-u}\text{Ba}_u\text{Mn}_{1-y}\text{Ti}_y\text{O}_3$ compositions, determined based on the PPMS data. On each experimental dependence, denoted with the same symbols as in Fig. 1, the fitted theoretical critical dependence (2), taking into account higher order terms, plotted with the thick red solid line, as well as the fitted Lorentz function, plotted with the thin black dashed line, are superimposed. Above each experimental curve, the u and y values, as well as the value, in parentheses, by which this curve was shifted along the vertical axis to maintain readability, are given.

phase transition, chosen judiciously for each composition. It should be mentioned that our trials to exclude the α parameter from the fitting process and to keep its value close to the values determined theoretically for most popular models (Ising, Heisenberg) did not give satisfactory results, and we were forced to treat α as the free, fitted parameter. During the analysis of the main magnetic phase, when choosing the temperature range for fitting, we considered the width of the anomaly and the necessity of minimizing the influence of a small amount of a parasitic phase, visible near 120 K as a small maximum on the low-temperature side of the specific heat anomaly for majority of the compositions. As it is shown in Fig. 4 with the thick solid lines, the shape of the specific heat anomaly related to the magnetic phase transition can be reproduced very well with Eq. (2) for all the compositions.

The values of the fitted parameters giving the best description of the experimental data are given in Table II. Uncertainty of each of these parameters was estimated by keeping all other parameters fixed and varying the investigated parameter up to the value for which a noticeable change of the fitted curve was observed. For completeness, the D^+ parameter, not fitted but calculated according to Eq. (3), is also given in the table. To differentiate the fitted T_N value from the value determined experimentally as the temperature at which the

specific heat anomaly reaches maximum and given in the last column of the table, the superscript “cr” was added to the former. Since in this analysis the seven parameters were fitted, the α values given in Table II cannot be treated as the real, accurately determined values of the critical exponent. In fact, the performed analysis allows us only to draw the conclusion that the α parameter is negative for the considered system.

Figure 4 shows that for the Ti-free compositions ($y = 0$) the anomaly related to the antiferromagnetic transition is asymmetric and λ -shaped, which is typical of the second-order transitions, whereas with partial replacement of the Mn ions with Ti ions, the anomaly becomes more symmetric as is observed in the case of the first-order transitions. To demonstrate this effect, we fitted the Lorentz function,

$$L(T) = \frac{L_0 w^2}{4(T - T_N^L)^2 + w^2}, \quad (4)$$

to the experimental data for the same temperature ranges as that used for fitting by Eq. (2). The fitted Lorentz functions are plotted in Fig. 4 using thin dashed lines, and the fitting parameters L_0 , w , and T_N^L are given in Table II. Like in the case of matching with Eq. (2), the uncertainty of each of the fitted parameters was estimated by keeping all other parameters fixed

TABLE II. Parameters of the theoretical function (2) and the Lorentz function (4) for which the best fit to the experimental specific heat anomalies related to the antiferromagnetic transition for the $\text{Sr}_{1-u}\text{Ba}_u\text{Mn}_{1-y}\text{Ti}_y\text{O}_3$ compositions was achieved.

Sample		α	B^-	B^+	E^-	E^+	D^-	D^+	T_N^{cr}	L_0	w	T_N^L	T_N
u	y		[J/(mole K)]				[J/(mole K)]		(K)	($\frac{\text{J}}{\text{mole K}}$)	(K)	(K)	(K)
0.5	0.1	-0.311(1)	9.68(2)	17(1)	1.64(2)	2.07(2)	-22.87(2)	-46(3)	168.9(2)	6.5(1)	28(1)	170.2(5)	170.2(5)
0.65	0.06	-0.76(1)	13.4(1)	13.4(2)	-0.003(3)	-0.22(4)	-7.36(6)	-7.4(5)	135.9(5)	8.80(5)	50.8(1)	132.5(1)	135.2(5)
										0.8(1)	3.7(4)	118.1(1)	
0.6	0.06	-0.574(1)	21.07(2)	26.1(5)	0.54(1)	0.53(1)	-27.24(2)	-36.0(9)	147.7(2)	9.17(5)	27.8(8)	146.6(5)	147.7(5)
0.55	0.06	-0.645(3)	16.43(5)	17.4(4)	0.35(1)	0.22(2)	-18.12(6)	-19.7(8)	163.7(5)	6.97(5)	30.7(7)	161.4(4)	163.3(5)
0.5	0.06	-1.25(1)	24.2(2)	9.1(2)	-0.49(2)	-1.82(3)	-11.4(2)	0.68(62)	161.0(8)	6.0(1)	33.6(9)	159.4(9)	160.5(5)
0.45	0.06	-0.80(1)	21.9(2)	5.4(1)	-0.27(2)	-3.48(5)	-15.5(2)	5.1(9)	186.8(5)	9.3(2)	34(2)	184(1)	186.0(5)
0.5	0.02	-0.90(5)	11.3(5)	11.9(2)	-2.92(5)	-3.08(5)	5.4(2)	4.7(9)	177.0(5)	13.4(2)	29(2)	175.7(6)	177.1(5)
0.45	0	-0.76(3)	15.7(3)	25.4(6)	-1.14(3)	-0.87(3)	-3.5(2)	-16(2)	193.7(5)	12.6(5)	31(2)	190(1)	193.5(5)
0.43	0	-0.66(1)	19.9(2)	26.0(8)	-0.48(4)	-0.56(3)	-13.4(2)	-23(2)	199.6(5)	12.7(5)	28(2)	196(1)	199.7(5)
0	0	-0.305(5)	9.83(7)	6.39(5)	0.23(5)	-1.86(4)	-9.7(1)	1.6(7)	228.0(5)	14.0(5)	39(2)	224(1)	228.1(5)

and varying the investigated parameter up to the value for which a noticeable change of the fitted curve was observed. Since for the sample with composition $u = 0.65$, $y = 0.06$ the additional maximum related to small content of an unknown parasitic phase was located very close to the main maximum on its low-temperature side, this composition was treated in a different way, i.e., the experimental maximum was described as a sum of two Lorentz functions, the first, which approximated the main anomaly, and the second, which estimated the parasitic anomaly. This approach reproduced quite well the shape of the combined anomaly, and the fitted parameters of the two Lorentz functions are given in Table II.

We noticed that for many Ti-containing compositions, the Lorentz function describes the specific heat anomaly nearly as well as the curve calculated with Eq. (2). To evaluate this observation quantitatively, we considered an average square of residuals per one point, defined by the formula

$$\sigma_f^2 = \frac{1}{N} \sum_{i=1}^N [y_i^{ex} - f(x_i^{ex})]^2, \quad (5)$$

where f denotes the investigated theoretical function and the summation extends over all N experimental points (x_i^{ex}, y_i^{ex}) for which the fitting was performed. This value has been calculated by taking as f the $C_M(T)$ function given by (2) and by taking as f the Lorentz function (4). Next, we plotted the difference between σ_L^2 and σ_{CM}^2 normalized to σ_{CM}^2 as a function of the composition, identified by the parameter $10y + u$, in Fig. 5. Clearly, with an increase in the Ti content the specific heat anomaly becomes more symmetric as is expected for the case of a first-order transition. In fact, with exception of the composition $u = 0.5$, $y = 0.06$, for which the Lorentz function describes the anomaly better, for all other compositions the description by Eq. (2) is better. However, in our opinion, it is not related to the real physical effect but to the fact that the fits of Eq. (2) were done with the larger number of free parameters.

Tentatively, the observed change of the shape of the specific heat anomaly can be elucidated by two scenarios.

According to the first one (in our opinion less probable), it can be ascribed to the disorder frozen below the ferroelectric transition and to the appearance of a Griffiths phase above

the magnetic transition. Indeed, the presence of the Griffiths phase was reported for several families of manganites [24] of a general composition AMnO_3 ; however, it was always related to a certain competition between different phases or interactions of different character. For example, in the idealized view, in the manganites of the type $(\text{La}^{3+}, \text{Sr}^{2+})(\text{Mn}^{3+}, \text{Mn}^{4+})\text{O}_3^{2-}$ [25], the 2+ and 3+ ions distributed randomly over the sublattice A cause that we have Jahn-Teller active Mn^{3+} and Jahn-Teller inactive Mn^{4+} ions distributed randomly over the Mn sublattice. Thus, the Mn subsystem is built of Jahn-Teller distorted and nondistorted Mn-O_6 octahedra, and if the neighboring Mn ions are of different valence, the ferromagnetic double exchange interaction between them dominates, whereas if the neighboring Mn ions are of the same valence, the antiferromagnetic superexchange interactions between them dominate. As the result, above the magnetic transition temperature, the Griffiths phase built of ferromagnetically and antiferromagnetically correlated microregions as well as paramagnetic microregions can exist in the sample.

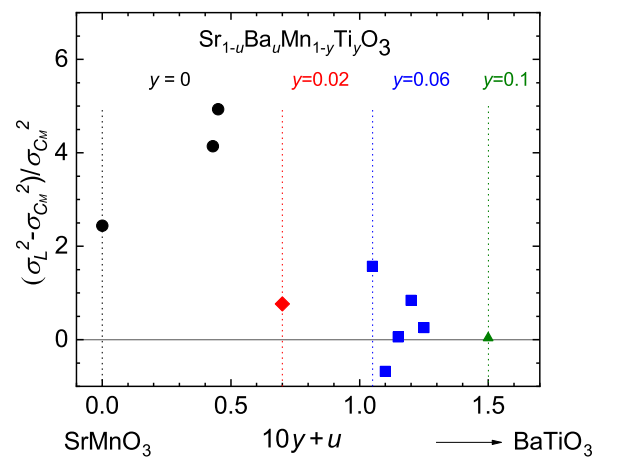


FIG. 5. Difference between average square of residuals corresponding to the Lorentz function and the critical behavior of Eq. (2) fittings as a function of composition. The arrow indicates the hypothetical composition to which the compositions studied evolve.

Similarly, in the other class of manganites, to which, for example, $(\text{Eu}^{3+}, \text{R}^{3+})\text{Mn}^{3+}\text{O}_3^{2-}$ compounds (R denotes a rare earth ion) belong, the Griffiths phase can exist [26]. In this class, the A sublattice is formed by isovalent $3+$ ions, which means that all Mn ions remain in the $3+$, Jahn-Teller active state. However, the Mn^{3+} ions have on their partially filled $3d$ shell four electrons, three of which occupy the t_{2g} states, whereas the fourth electron has for its disposal two orbitals, theoretically, of the e_g type. Actually, denotations e_g and t_{2g} refer to orbitals that form in the octahedral environment. However, due to the Jahn-Teller effect, the octahedral environment of the Mn ion deforms, and a few different forms of the deformation are equivalent energetically. Thus, instead of the two pure e_g orbitals we have two different linear combinations of them for each form of the Jahn-Teller deformation. The e_g -type orbital of lower energy, occupied by the fourth electron, is elongated along different axis for different type of the deformation. As the result, denoting different types of the deformation by subscripts “I” and “II,” if the bonding between two neighboring Mn ions has a form $\text{Mn}_\text{I}^{3+}-\text{O}^{2-}-\text{Mn}_\text{II}^{3+}$, the superexchange interaction between them has, usually, the ferromagnetic character [27], whereas if the bonding between two neighboring Mn ions has a $\text{Mn}_\text{I}^{3+}-\text{O}^{2-}-\text{Mn}_\text{I}^{3+}$ or $\text{Mn}_\text{II}^{3+}-\text{O}^{2-}-\text{Mn}_\text{II}^{3+}$ form, the superexchange interactions between them have the antiferromagnetic character. Thus, in such materials, above the magnetic transition temperature, regions with dominating ferromagnetic correlations can neighbor on regions with dominating antiferromagnetic correlations and the Griffiths phase can be formed.

The case of compositions studied in the present paper is different. Their A sublattice is formed by $2+$ ions only (Sr^{2+} and Ba^{2+}); thus, the Mn sublattice is made of the Jahn-Teller inactive Mn^{4+} ions only. As the result, all superexchange interactions along the paths $\text{Mn}^{4+}-\text{O}^{2-}-\text{Mn}^{4+}$ are antiferromagnetic, and no competition with ferromagnetic interactions appears. As the only origin of appearance of the Griffiths phase, the dilution of the tetragonal network of the Mn^{4+} magnetic ions with nonmagnetic Ti^{4+} ions could be indicated. Such a diluted network was a subject of the fundamental Griffiths work [28], in which the phenomenon of correlated clusters embedded in the nonordered medium was considered. However, this phenomenon appears usually, when the dilution level is close to the percolation threshold. For the case of a simple cubic lattice of magnetic ions the percolation threshold appears at ~ 0.31 occupied sites [29]. Assuming that the threshold for the simple tetragonal lattice existing in our compounds is not substantially different, we can state that our system, which has not fewer than 0.9 occupied magnetic sites (the highest level of Ti substitution in our samples is 0.1), is too dense to show properties of rare lattice. Thus, we realize that the observed change of the shape of specific heat anomaly rather should not be ascribed to the frozen disorder or to the Griffiths phase.

In our opinion, the other scenario, related to the mechanism analyzed in Ref. [14] is more appropriate. The authors of Ref. [14] considered a classical ferromagnetic system, showing the second-order transition between the paramagnetic and ferromagnetic phases at T_C , within the molecular field approximation. They showed that if in such a system, the exchange integral, usually assumed to be constant, is a

function of temperature (or indirectly, if it is a function of volume being a function of temperature), then the temperature dependence of the order parameter will be steeper than that given by a classical critical relation $(T - T_C)^{-\beta}$, and eventually, for sufficiently strong temperature dependence of the exchange integral, characterized by a parameter η , the transition becomes the first-order transition, at which a jump of the order parameter from a certain small value to zero takes place. (It can be mentioned that such first-order transitions, for which an order parameter can be defined, which decreases on approaching the transition, then shows a jump to zero at the transition point, and then its short-range correlations can be observed above the transition point, are sometimes called the first-order transitions close to the second-order ones. If the short-range fluctuations of the order parameter above the transition can be neglected, such transitions can be considered theoretically within the molecular field approximation or in frames of the Landau model by adding the term proportional to the third power of the order parameter to the expansion of the thermodynamic potential [24].)

Considering the above mechanism in the context of the $(\text{Sr},\text{Ba})(\text{Mn},\text{Ti})\text{O}_3$ system, showing the antiferromagnetic transition, we see that it was evidenced experimentally [10–13] that the ferroelectric, tetragonal distortion of the crystal lattice decreases with lowering temperature and changes substantially on approaching the Néel temperature. Taking into account that the decrease in distortion is correlated with the decrease of the displacement of the Mn ions from the central position within the $\text{Mn}-\text{O}_6$ octahedra, this decrease is inevitably related to changes of the Mn-O bond lengths and Mn-O-Mn bond angles. As was shown, e.g., in [30], changes in these parameters influence strongly the value of the superexchange constants. Thus, formally, the basic assumption of the model [14] is fulfilled; however, it is not clear whether the change in the superexchange constants is sufficiently strong to change the order of the transition. At the same time, the literature data on the temperature dependence of the antiferromagnetic order parameter are equivocal. For example, in Fig. 11(b) of Ref. [13], presenting the temperature dependence of muon fast relaxation time, being proportional to the antiferromagnetic order parameter, we can notice much steeper dependence with a possible jump to zero for the composition containing 0.05 Ti in comparison with the Ti-free composition, which supplies the argument in favor of the scenario considered. Also the temperature dependence of the average magnetic moment of the Mn^{4+} ion for the compound containing 0.07 Ti, determined from the neutron diffraction data and presented in the inset to Fig. 2(a) of Ref. [12], does not follow the classical critical dependence and does not exclude the presence of a small jump of the magnetic order parameter to zero, which also does not contradict the considered interpretation. On the other hand, Fig. S3 from the supplementary material of Ref. [12], presents temperature dependence of the integrated intensity of the $(1/2\ 1/2\ 1/2)$ neutron magnetic reflection for the composition containing 0.07 Ti, which seems to follow the classical critical dependence; however, the low-temperature part of this dependence shows rather unphysical lowering of this intensity, and the temperature scale of the figure does not emphasize the behavior within a narrow critical range. Moreover, the technological

difficulties in preparing the Ti-containing compositions, mentioned above, can result in small inhomogeneities of the chemical composition of some samples. Based on these facts, we can state that it is difficult to notice a small jump in the antiferromagnetic order parameter in its experimental studies.

However, in the case of the first-order transition, the jump in the order parameter is inevitably accompanied by a jump in entropy, S , which is responsible for the effect of the latent heat. Thus, taking into account that the Dirac δ function is the derivative of the step, i.e., Heaviside, function, the specific heat, which is proportional to the derivative of entropy, $C = T(dS/dT)$, should be the quantity much more sensitive to the presence of a step change in entropy, showing a huge, symmetric anomaly at the first-order transition point. Since in the real systems, the first-order transition can be accompanied by thermal hysteresis (this effect was not observed in the studied system), and it can go through the state of coexistence of both phases, the real anomaly is usually wider and rounded in comparison with the δ function, thus we approximated its shape with the Lorentz function. As was mentioned above, with increase of the Ti content, the specific heat anomaly at the magnetic transition becomes more symmetric and better described by the Lorentz function. This suggests that, in spite of the earlier suggestions [12,13], the antiferromagnetic transition in the (Sr,Ba)(Mn,Ti)O₃ system changes its character from the second- to the first-order one with increase in the Ti content. However, in order to make a decisive statement, it would be necessary to formulate the Bean-Rodbell model [14] and to define a parameter analogous to η for the case of the antiferromagnetic material, as well as to calculate, whether the temperature changes of the superexchange integrals are sufficiently strong to induce the change of the phase transition order.

V. CONCLUSIONS

Our specific heat studies of the (Sr,Ba)(Mn,Ti)O₃ compounds showed that the anomalies accompanying the antiferromagnetic transition are spread over the wide temperature range of 160 ± 50 K. Thus, under the assumption that this is the second-order transition, the critical behavior of the specific heat must be analyzed in frames of the more advanced theory than usually, i.e., within theory taking into account higher order terms in expansion of the free energy. Parameters of such critical behavior were determined. However, it was observed that with the increase of Ti content, the specific heat anomalies change their λ shape by becoming more symmetric and can be approximated by the Lorentz function, which suggests that, in spite of the earlier predictions [12,13], the transition changes its character from the second-order to the first-order one.

It was shown by the DSC studies that the ferroelectric phase transition [11,12] appearing, in dependence on the composition, within the range 350–400 K is accompanied, for a majority of the compositions, by a smeared and not well-pronounced anomaly in the temperature dependence of specific heat. We attribute this fact tentatively to the wide temperature hysteresis of this transition [11,12] and presence of the nanoscale tetragonal distortions in the paraelectric phase [13], which causes the transition to go through the phase coexistence state over a large temperature interval. Moreover, a small difference between entropies of the para- and ferroelectric phases can deteriorate the visibility of the specific heat anomaly.

ACKNOWLEDGMENTS

This work was supported partially by the National Science Centre, Poland, under Project No. 2018/31/B/ST5/03024.

- [1] H. Schmid, Multi-ferroic magnetoelectrics, *Ferroelectrics* **162**, 317 (1994).
- [2] D. Khomskii, Classifying multiferroics: Mechanisms and effects, *Physics* **2**, 20 (2009).
- [3] P. Barone and S. Picozzi, Mechanisms and origin of multiferroicity, *C. R. Physique* **16**, 143 (2015).
- [4] M. Kenzelmann, A. B. Harris, S. Jonas, C. Broholm, J. Schefer, S. B. Kim, C. L. Zhang, S.-W. Cheong, O. P. Vajk, and J. W. Lynn, Magnetic inversion symmetry breaking and ferroelectricity in TbMnO₃, *Phys. Rev. Lett.* **95**, 087206 (2005).
- [5] S.-W. Cheong and M. Mostovoy, Multiferroics: A magnetic twist for ferroelectricity, *Nat. Mater.* **6**, 13 (2007).
- [6] T. Kimura, T. Goto, H. Shintani, K. Ishizaka, T. Arima, and Y. Tokura, Magnetic control of ferroelectric polarization, *Nature (London)* **426**, 55 (2003).
- [7] A. P. Pyatakov and A. K. Zvezdin, Magnetoelectric and multiferroic media, *Phys. Usp.* **55**, 557 (2012).
- [8] D. I. Khomskii, Multiferroics: Different ways to combine magnetism and ferroelectricity, *J. Magn. Magn. Mater.* **306**, 1 (2006).
- [9] I. A. Sergienko and E. Dagotto, Role of the Dzyaloshinskii-Moriya interaction in multiferroic perovskites, *Phys. Rev. B* **73**, 094434 (2006).
- [10] H. Sakai, J. Fujioka, T. Fukuda, D. Okuyama, D. Hashizume, F. Kagawa, H. Nakao, Y. Murakami, T. Arima, A. Q. R. Baron *et al.*, Displacement-type ferroelectricity with off-center magnetic ions in perovskite Sr_{1-x}Ba_xMnO₃, *Phys. Rev. Lett.* **107**, 137601 (2011).
- [11] H. Somaïly, S. Kolesnik, J. Mais, D. Brown, K. Chapagain, B. Dabrowski, and O. Chmaissem, Strain-induced tetragonal distortions and multiferroic properties in polycrystalline Sr_{1-x}Ba_xMnO₃ ($x = 0.43-0.45$) perovskites, *Phys. Rev. Mater.* **2**, 054408 (2018).
- [12] K. Chapagain, D. E. Brown, S. Kolesnik, S. Lapidus, B. Haberl, J. Molaison, C. Lin, C. Kenney-Benson, C. Park, J. Pietosa *et al.*, Tunable multiferroic order parameters in Sr_{1-x}Ba_xMn_{1-y}Ti_yO₃, *Phys. Rev. Mater.* **3**, 084401 (2019).
- [13] B. Jones, C. Z. Suggs, E. Kriviyakina, D. Phelan, V. O. Garlea, O. Chmaissem, and B. A. Frandsen, Local atomic and magnetic structure of multiferroic (Sr,Ba)(Mn,Ti)O₃, *Phys. Rev. B* **109**, 024423 (2024).
- [14] C. P. Bean and D. S. Rodbell, Magnetic disorder as a first-order phase transformation, *Phys. Rev.* **126**, 104 (1962).
- [15] A. Oleaga, A. Salazar, D. Prabhakaran, J.-G. Cheng, and J.-S. Zhou, Critical behavior of the paramagnetic to antiferromagnetic transition in orthorhombic and hexagonal phases of

- RMnO_3 ($R = \text{Sm, Tb, Dy, Ho, Er, Tm, Yb, Lu, Y}$), *Phys. Rev. B* **85**, 184425 (2012).
- [16] T. Zajarniuk, A. Szewczyk, P. Wisniewski, M. U. Gutowska, R. Puzniak, H. Szymczak, I. Gudim, V. A. Bedarev, M. I. Pashchenko, P. Tomczak, and W. Szuszkiewicz, Quantum versus classical nature of the low-temperature magnetic phase transition in $\text{TbAl}_3(\text{BO}_3)_4$, *Phys. Rev. B* **105**, 094418 (2022).
- [17] J. Wieckowski, M. U. Gutowska, A. Szewczyk, S. Lewinska, K. Conder, E. Pomjakushina, V. P. Gnezdilov, and S. L. Gnatchenko, Thermal properties of layered cobaltites $\text{RBaCo}_2\text{O}_{5.5}$ ($R = \text{Y, Gd, and Tb}$), *Phys. Rev. B* **86**, 054404 (2012).
- [18] C. A. Martin, Simple treatment of anharmonic effects on the specific heat, *J. Phys.: Condens. Matter* **3**, 5967 (1991).
- [19] F. J. Wegner, Corrections to scaling laws, *Phys. Rev. B* **5**, 4529 (1972).
- [20] G. Ahlers and A. Kornblit, Universality of the specific heat of Heisenberg magnets near the critical temperature, *Phys. Rev. B* **12**, 1938 (1975).
- [21] A. Kornblit and G. Ahlers, Heat capacity of RbMnF near the antiferromagnetic transition temperature, *Phys. Rev. B* **8**, 5163 (1973).
- [22] A. Kornblit and G. Ahlers, Heat capacity of EuO near the Curie temperature, *Phys. Rev. B* **11**, 2678 (1975).
- [23] J. J. Binney, N. J. Dowrick, A. J. Fisher, and M. E. J. Newman, *The Theory of Critical Phenomena: An Introduction to the Renormalization Group* (Clarendon Press, Oxford, 1992).
- [24] T. Vojta, Rare region effects at classical, quantum and nonequilibrium phase transitions, *J. Phys. A: Math. Gen.* **39**, R143 (2006).
- [25] J. Deisenhofer, D. Braak, H.-A. Krug von Nidda, J. Hemberger, R. M. Eremina, V. A. Ivanshin, A. M. Balbashov, G. Jug, A. Loidl, T. Kimura, and Y. Tokura, Observation of a Griffiths phase in paramagnetic $\text{La}_{1-x}\text{Sr}_x\text{MnO}_3$, *Phys. Rev. Lett.* **95**, 257202 (2005).
- [26] A. Karmakar, S. Majumdar, S. Kundu, T. K. Nath, and S. Giri, A Griffiths-like phase in antiferromagnetic $\text{R}_{0.5}\text{Eu}_{0.5}\text{MnO}_3$ ($R = \text{Pr, Nd, Sm}$), *J. Phys.: Condens. Matter* **25**, 066006 (2013).
- [27] E. Dagotto, T. Hotta, and A. Moreo, Colossal magnetoresistant materials: The key role of phase separation, *Phys. Rep.* **344**, 1 (2001).
- [28] R. B. Griffiths, Nonanalytic behavior above the critical point in a random Ising ferromagnet, *Phys. Rev. Lett.* **23**, 17 (1969).
- [29] A. Sur, J. L. Lebowitz, J. Marro, M. H. Kalos, and S. Kirkpatrick, Monte Carlo studies of percolation phenomena for a simple cubic lattice, *J. Stat. Phys.* **15**, 345 (1976).
- [30] J. B. Goodenough, Electronic and ionic transport properties and other physical aspects of perovskites, *Rep. Prog. Phys.* **67**, 1915 (2004).